Effect of hydroxyapatite size on properties of PBS-DLS/HAp composites obtained by twin-screw extrusion and injection moulding techniques

Kryszak Bartłomiej[1]*, Zarei Moein[2], Biernat Monika[3], Szterner Piotr[3], Pagacz Joanna[4], Tymowicz-Grzyb Paulina[4], Antosik Agnieszka[4], Gąsiński Arkadiusz[4], Szustakiewicz Konrad[1], El Fray Mirosława[2]

[1] Department of Polymer Engineering and Technology, Faculty of Chemistry, Wrocław University of Science and Technology (WUST), Wyb. Wyspiańskiego 27, 50-370 Wrocław, Poland.
[2] Department of Polymer and Biomaterials Science, Faculty of Chemical Technology and Engineering, West Pomeranian University of Technology in Szczecin, Al. Piastow 45, 71-311 Szczecin, Poland
[3] Biomaterials Research Group, Łukasiewicz Research Network, Institute of Ceramics and Building Materials, Cementowa 8, 31-983 Cracow, Poland
[4] Ceramics Research Group, Łukasiewicz Research Network - Institute of Ceramics and Building Materials, Cementowa 8, 31-983 Cracow, Poland

ABSTRACT

The aim of this work is to develop new polymer-ceramic composites based on poly(butylene succinate-dilinoleic succinate) (PBS-DLS) and hydroxyapatites (HAp) of different sizes. Irregularly shaped nano-hydroxyapatite (nHAp) and whisker-shaped micro-hydroxyapatite (μHAp) were used as fillers. For each of the hydroxyapatites, composites with copolymer:filler weight ratios of 9:1 and 8:2 were prepared by co-rotating twin-screw extrusion combined with injection moulding techniques. The investigations carried out allowed the characterisation of the specific behaviour of both fillers during processing, such as the tendency of nanoparticles to agglomerate or the breaking of whisker microparticles leading to a significant change in their aspect ratio (from about 4 to less than 3). A comprehensive characterisation of the produced materials was carried out and a comparison was made of the effect of filler particle size on the physicochemical and mechanical properties of the composites. A series of mechanical tests were carried out, such as dynamic thermo-mechanical analysis, quasi-static tensile test, quasi-static flexural test, impact strength and Brinell hardness, showing the reinforcing effect of the fillers used, with a predominance of whiskered micro-hydroxyapatite. The developed materials also showed good processability, thermal stability, bioactivity and biocompatibility towards the mouse fibroblast L929 cell line. The results presented in this work certainly provide useful information for the design and fabrication of effective polymer-ceramic biocomposites for bone tissue engineering applications.

Keywords

poly(butylene succinate), hydroxyapatite whiskers, nano-hydroxyapatite, injection molding, mechanical properties

1. Introduction

Biodegradable polymers have gained a lot of interest in recent decades. Their ability to biodegrade under natural environmental conditions, combined with their biological safety, has led to their increasing use in various areas of our lives, such as the packaging industry, agriculture, geotextiles, pharmaceuticals or medicine [1,2]. A growing field of application for such polymers is biomaterial applications which are directly related to the regeneration or 'repair' of human tissues. The term of ‘biomaterials’ is used to describe, for example, drug carriers, tissue scaffolds or other biomedical devices such as sutures, pins, meshes or tissue-stabilising elements [1,3]. Among the biodegradable polymers, aliphatic polyesters, such as polylactide (PLA), poly(lactide-co-glycolide) (PLGA) or polycaprolactone (PCL), are a prominent group, characterised by good mechanical parameters, consistent properties and biocompatibility [4]. In recent years, the popularity of another representative of this group - poly(butylene succinate) (PBS) – has increased. This popularity is related

https://doi.org/10.26434/chemrxiv-2024-6nlfd **ORCID:** https://orcid.org/0000-0001-9807-964X Content not peer-reviewed by ChemRxiv. **License:** CC BY 4.0

to its excellent biocompatibility, reasonably balanced thermo-mechanical properties and very good thermo-processability [5].

One of the main drawbacks of PBS compared to other better known aliphatic polyesters is its poor mechanical properties including the high brittleness. In order to extend its applicability, many modifications have been developed, including blending, copolymerisation with suitable monomeric units and composite formulation [5]. One of the most widely studied PBS-based blends are PLA/PBS systems [6,7]. The studies included in these works indicate an increase in mechanical parameters (tensile modulus, tensile strength) in proportion to the increase in PLA content in the system with a concomitant loss of ductility. Several PBS-based copolymers have also been reported in the literature. Very often these are multi-block copolymers containing, in addition to PBS, the so-called soft segments such as saturated dilinoleic acid (DLA) [8] or dilinoleic succinate (DLS) [9,10]. Increasing the amount of soft segments in the copolymer improves the flexibility of the polymer chains, which is reflected in the properties of the material. To date, many more complex systems have been developed, such as PBS-DLS-PEG, which allows the modification of properties such as hydrophilicity (thanks to the introduction of the poly(ethylene glycol) (PEG) segment) [11].

As mentioned above, the improvement of the performance properties of PBS-based materials can be achieved by creating a composite system. To date, additives such as lignin [12], cellulose [13], chitin [14] or hydroxyapatite (HAp) particles [14–17] have been used. The last of these fillers - HAp - is a mineral with a composition similar to the mineral fraction of human bone, making it a candidate for use in bone tissue engineering [18]. To date, several experiments have been carried out using PBS-based materials with the addition of HAp. Piotr Prowans et al. showed that the PBS-DLA composite with 30 wt% addition of hydroxyapatite nanoparticles is an attractive material for bone healing applications [17]. In turn, GanG Li's work demonstrated that the addition of HAp nanoparticles to PBS significantly improved the proliferation and adhesion of mouse embryonic fibroblast cells to the surface of the porous biomaterial [16]. Studies have also been carried out demonstrating the reinforcing effect of HAp nanoparticles on the mechanical properties of PBS-based materials prepared by extrusion and injection moulding methods. In all of these works, nano-sized HAp particles were used. To date, there are no reports on the influence of micro-hydroxyapatite on the broadly understood properties of PBS-based materials. Many scientific reports indicate that the particle size of the apatite filler can have a significant effect on biological, physicochemical or mechanical properties [19–23].

In view of the above, the work involved the preparation of new PBS-DLS composites with the addition of hydroxyapatite using twin screw extrusion and injection moulding techniques. A comparative analysis of the physicochemical and mechanical properties of two series of materials differing in the size and shape of the HAp filler particles was carried out. Nanometric hydroxyapatite with irregular filler grain shape and micrometric hydroxyapatite with needle/whisker shape were used for the investigation. This is the first time such an analysis has been reported for PBS-based materials.

2. Methodology

2.1. Materials

2.1.1. PBS-DLS copolymer

Poly(butylene succinate-dilinoleic succinate) (PBS-DLS) copolyester with a hard to soft segment ratio of 90:10 by weight was used for the research. The synthesis procedure is reported in [10].

2.1.2. Hydroxyapatites

Hydroxyapatites (nHAp and μHAp) with two types of morphology were prepared from the following substrates: calcium hydroxide $Ca(OH)_2$ (CAS:1305-62-0, pure p.a. Chempur, PL), ortho-phosphoric acid H_3PO_4, 85% (CAS:7664-38-2, pure p.a. Chempur, PL), ammonia NH_4OH 25% (CAS: 1336-21-6, pure p.a. Chempur, PL), calcium nitrate tetrahydrate $Ca(NO_3)_2{\cdot}4H_2O$ (CAS:13477-34-4, pure p.a. Chempur, PL),

https://doi.org/10.26434/chemrxiv-2024-6nlfd **ORCID:** https://orcid.org/0000-0001-9807-964X Content not peer-reviewed by ChemRxiv. **License:** CC BY 4.0

sodium dihydrogen phosphate NaH_2PO_4 (CAS:7558-80-7, pure p.a. Chempur, PL), urea CH_4N_2O (CAS: 57-13-6, pure p.a. Chempur, PL).

Nanohydroxyapatite $Ca_{10}(PO_4)_6(OH)_2$ was synthesised by the aqueous precipitation method from calcium hydroxide and orthophosphoric acid added dropwise over 45 min with constant stirring under alkaline conditions (pH=11) by adding ammonia solution, if necessary. Appropriate amounts of substrates with a Ca/P molar ratio of 1,67 were used. The synthesis was carried out at 50 °C for 2 h. The precipitate was rinsed 4 times with deionised water and centrifuged (3700 rpm for 3 min) until the excess ammonia solution was removed. The resulting nanoHAp was dried at 90 °C for 24 h.

The synthesis of µHAp particles was carried out by homogenous precipitation method. The main substrates used for the synthesis of the HAp were: calcium nitrate tetrahydrate, sodium dihydrogen phosphate and urea for pH control. The appropriate amounts of substrates with Ca/P molar ratio of 1,67 were mixed with deionised water in a three-necked flask with a reflux condenser. The synthesis was carried out at 90 °C for 48 h. Finally, the precipitated solid phase obtained was washed with boiling distilled water and dried at 90 °C for 24 h.

The use of two different synthesis methods resulted in products with different morphologies (irregular-shaped nanohydroxyapatite (Fig.1a) and microfibrous (whisker-shaped) hydroxyapatite (Fig. 1b)). The exact particle size characterisation of both fillers is given in section 3.2. Both products obtained were characterized by X-ray powder diffraction as a single phase (100% of hydroxyapatite) (Fig. S1). However, the hydroxyapatite particles obtained differed in the size of the specific surface area (BET). Clearly, the nanohydroxyapatite particles exhibited a significantly larger specific surface area (S_{BET} = 80.68 ± 0.12 m²/g) than the micrometric particles (S_{BET} = 5.73 ± 0.02 m²/g). The size ratio of the specific surface area of nHAp/µHap is approximately 14.

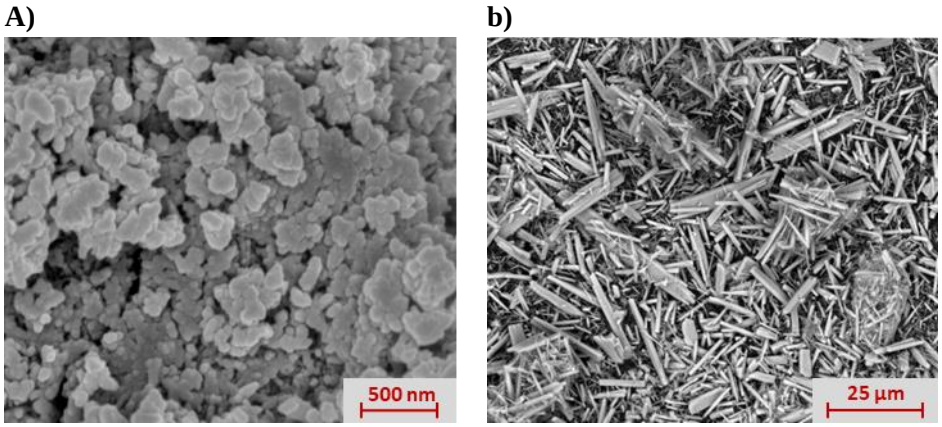

Figure 1. SEM images of hydroxyapatite powders used in the work: a) nHAp, b) µHAp.

2.1.3. Composites preparation

Two series of polymer-ceramic composites were produced, differing in the geometry of the hydroxyapatite filler particles. Within each series, two systems were prepared with polymer/filler weight ratios of 9/1 and 8/2. An unfilled copolymer sample was prepared as a reference. Table 1 shows each of the systems together with the nomenclature used in the work.

The manufacturing process consisted of three main steps. First, the input polymer and HAp powders were dried to remove moisture from the structure. The next step was twin-screw extrusion to achieve the best possible dispersion of the filler in the system. The final step, after granulation of the extruded material, was injection moulding to give the final shape to the material.

The drying step of the materials was carried out in separate vacuum dryers for 24 hours at a temperature of 100 ºC (HAp powders) or 60 ºC (polymer granules). The extrusion process was carried out using a Thermo Fisher Scientific twin-screw extruder (D = 20 mm, L/D = 40) at a screw rotational speed of 200 rpm and a barrel temperature of 125 °C. The extrudates were collected using a Thermo Scientific filament winding system

https://doi.org/10.26434/chemrxiv-2024-6nlfd **ORCID:** https://orcid.org/0000-0001-9807-964X Content not peer-reviewed by ChemRxiv. **License:** CC BY 4.0

at a speed of approximately 1 m/min. Finally, the extruded materials were granulated using a Brabender pelletiser and then moulded using a BOY XS micro-injection molding machine. All materials were injected under similar conditions, with a temperature of 130 ºC in all heating zones and a pressure of 150 bar. The mould cooling temperature was 40 ºC, and the total duration of a single injection cycle was approximately 20 seconds.

Finally, three types of specimens were obtained for each material: dumbbell-shaped specimens for tensile tests (type 5A according to PN-EN ISO 527), rectangular beams for dynamic impact and static bending tests (80 mm x 10 mm x 4 mm), and 3 cm x 3 cm x 0.5 mm plates for other experiments.

Table 1. Names of the samples.

Sample's name	wt.% of PBS-DLS	wt.% of nHAp	wt.% of µHAp
coPBS	100	-	-
coPBS_10%nHAp	90	10	-
coPBS_20%nHAp	80	20	-
coPBS_10%µHAp	90	-	10
coPBS_20%µHAp	80	-	20

2.2. MATERIALS CHARCTERIZATION

2.2.1. Scanning electron microscopy (SEM)

Scanning electron microscopy (SEM) was carried out using a Nova NanoSEM 200, FEI. A high vacuum ETD detector (Everhart-Thornley) was used to determine the shape and size of the grains in the hydroxyapatite powders. To define the distribution of hydroxyapatite particles in the manufactured composites, a backscattered electron (BSE) detector was used in low vacuum conditions. Both detectors are combined with Nova NanoSEM 200, observations at 15 kV accelerating voltage.

2.2.2. Phase composition (XRD)

The phase composition of the HAp powders was determined using a Bruker-AXS D8 DAVINCI diffractometer equipped with Bragg-Brentano geometry and CuKα radiation. The XRD patterns were recorded from 5 to 120° in a 2θ scale with a step of 0.01° and a scan speed of 2 s per step. The crystalline phases were identified using the Crystallography Open Database (COD) and the DIFFRACplus EVA-SEARCH software.

2.2.3. Specific surface area (BET)

The Brunauer-Emmett-Teller (BET) method was used to evaluate the specific surface area of the hydroxyapatite samples using a Gemini VII 2390t Micromeritics analyser. The analysis was based on the determination of 9 points of nitrogen adsorption isotherm in the pressure range of 0.05–0.25 p/p°, where p and $p°$ are the equilibrium and the saturation pressures of adsorbates at the liquid nitrogen temperature, respectively. Prior to N_2 adsorption, the samples were degassed at 105 °C in the N_2 atmosphere for 1 h to dry and purify the samples.

2.2.4. Particle size distribution

The particle size distribution was estimated based on the approach described in our recent work [24]. The composite samples were calcined at 500 °C for 24 h under static conditions, to remove the polymer fraction from the system while preventing HAp degradation. Particle size distribution was analysed from the collected SEM images. Each image was processed using ImageJ software. Images were converted to 8-bit grey scale, then smoothed and segmented. Segmentation was based on finding local maxima on the images with a prominence of at least 10 (ion a scale of 0-255). The background was subtracted to obtain the final images of the separated particles. Several thousand of objects (particle images) per sample were obtained and subjected to automated size and shape analysis. For each object the area, perimeter, major and minor ellipse axes,

https://doi.org/10.26434/chemrxiv-2024-6nlfd ORCID: https://orcid.org/0000-0001-9807-964X Content not peer-reviewed by ChemRxiv. License: CC BY 4.0

circularity, aspect ratio and roundness were analysed. The area of each object was converted to equivalent diameter and then analysed in relation to the shape parameters using a custom written macro (Python language).

2.2.5. Gel permeation chromatography

Gel permeation chromatography (GPC) was used to study the average (apparent) molar mass (M_n and M_w) and molar mass dispersity (Đ) of the synthesised copolymers. The analysis was carried out using an HPLC Agilent 1200 series modular system with a refractive index detector (RID) which was equipped with two PLgel 5µm MIXED-C columns (300x7.5mm) connected in series. Samples were prepared in chloroform (CHCl3) at a concentration of 3mg/ml and filtered through a 0.2µm polytetrafluoroethylene (PTFE) membrane. Data were recorded using "ChemStation for LC" and analysed using "ChemStation GPC Data Analysis Software".

2.2.6. Material density

The absolute density of the materials was determined by the buoyancy method using a Hildebrand Electronic Densimeter H-300S. Measurements were taken at room temperature. The final density value of each material was reported as the average of 10 measurements.

2.2.7. Melt Mass-Flow Rate (MFR)

The mass melt flow rate parameters were determined using a Zwick Roell Mflow rheometer, in accordance with the ASTM D1238 standard. Prior to testing, the samples were dried under vacuum for 24 hours at 60 °C. Measurements were made under the same conditions for all materials, for a 6 g sample, at a temperature of 125 ºC and a load of 2.16 kg. The cut-off time was chosen individually for each of the samples and was in the range of 10-15 s. The *MFR* index was determined from equation 1.

$$MFR = \frac{600 \cdot M}{t} \left[\frac{g}{10\ min}\right] \qquad (1)$$

where *M* [g] - mass of material collected over time, *t* [s] - material flow time of mass *M*.

2.2.8. Thermogravimetry

The thermal stability of the prepared materials was analysed using a STA F3 449 Jupiter® Netzsch thermal analyser. Simultaneous TG–DTA experiments were performed under a dynamic flow of argon (70 mL/min) with samples without any pretreatment. Each sample of approximately 10 mg was heated from 30°C up to 700 °C at a heating rate of 10 °C/min in an Al_2O_3 DTA pan. Measurements were repeated twice for each sample.

2.2.9. Differential scanning calorimetry

The thermal properties of the copolymers were studied using differential scanning calorimetry (DSC). The samples were pretreated by keeping them in a vacuum oven at 45 °C for 24 hours, before being placed in aluminium pans and subjected to heating-cooling-heating cycles in a DSC Q2500 Discovery instrument from TA Instruments. The temperature range used was from -90 to 200 °C, at a heating rate of 10 °C/min. The data obtained were analysed using Trios software. The degree of crystallinity (X_C) of the materials was calculated using the formula described in the literature [25], taking into account that the system is a composite:

$$X_C = \frac{\Delta H_m}{W \cdot \Delta H_m^{100\%}} \cdot 100\%$$

where: ΔH_m – melting enthalpy of the material, $\Delta H_m^{100\%}$ – melting enthalpy of 100% crystalline PBS (110.3 J/g), W - weight fraction of copolymer in the composite.

https://doi.org/10.26434/chemrxiv-2024-6nlfd **ORCID:** https://orcid.org/0000-0001-9807-964X Content not peer-reviewed by ChemRxiv. **License:** CC BY 4.0

2.2.10. Dynamic mechanical thermal analysis (DMTA)

The dynamic thermomechanical tests were performed using a DMA/SDTA 1+ instrument from Mettler Toledo (Greifensee, Switzerland). Measurements were made in single cantilever mode on 30 mm × 4 mm × 2 mm specimens cut from the gauge length of tensile test specimens. First, a series of pre-tests (strain sweep measurements) were performed, to determine the linear viscoelastic region of the specimens tested. The actual viscoelastic measurements were performed in the temperature range of -80–120 °C at a heating rate of 3 °C/min, with a constant displacement amplitude of 20 µm and a frequency of 1 Hz. Finally, frequency sweep tests from 0.1 to 100 Hz were performed in the linear viscoelastic region for the same displacement amplitude at room temperature (25 ºC).

2.2.11. Quasi-static tensile test

The static tensile tests were carried out in accordance with EN ISO 527 using the universal tensile testing machine (Instron 5966) with a 10 kN head. Measurements were performed at 25 °C at the stretching rate of 100 mm/min. The characteristic strength parameters including ultimate tensile strength (*UTS*), Young's modulus (E) and strain at break (ε_B) were determined for each material using the Bluehill 3 software. The results obtained are the average values of approximately 10 measurements.

2.2.12. Quasi-static three-point bending test

The static bending tests were carried out in accordance with EN ISO 178 using a universal testing machine (Instron 5966) with a 10 kN head. The measurements were performed at 25 °C with a bending rate of 2 mm/min and the span length of 64 mm. The test was carried out on 80 mm x 10 mm x 4 mm injection moulded specimens. Using this technique, two characteristic parameters were determined: flexural modulus (E_B) and stress at 3.5% strain ($\sigma_{\varepsilon=3.5\%}$). The results obtained are the average values of approximately 10 measurements.

2.2.13. Charpy impact test

The dynamic impact test was performed in accordance with the EN ISO 13802 standard. A Charpy Zwick Roell HT5.5P pendulum hammer with a nominal impact energy of 0.5 J was used for the test. 10 mm x 80 mm x 2 mm test specimens were produced by injection moulding in accordance with the standard. The final stage in the production of the test specimens was the drilling a 2 mm deep notch using a Zwick Roell notching machine. This method was used to determine the parameter a_N - Charpy notched impact strength was determined. The value of this parameter was determined as the average of 10 measurements.

2.2.14. Hardness

Hardness measurements of the tested materials were carried out using a Brinell apparatus that complies with EN ISO 6506 equipped with a steel ball. The value of the hardness parameter (HB) was determined as the average of 10 measurements.

2.2.15. Bioactivity

To mimic physiological conditions, a simulated body fluid (SBF) was prepared according to the protocol of Kokubo et al. [26]. The solution was made by dissolving reagents such as NaCl, $NaHCO_3$, KCl, $K_2HPO_4 \cdot 3H_2O$, $MgCl_2 \cdot 6H_2O$, 1M-HCl, $CaCl_2$, Na_2SO_4, and $(CH_2OH)_3CNH_2$ in ion-exchanged and distilled water at 36.5 °C and adjusting the pH to 7.4 with 1N-HCl solution. The SBF was stored at 5 °C until use and was replaced with fresh solution once a week. Copolymer films with a thickness of 0.5 mm and dimensions of 15x15 mm were immersed in the SBF and kept in dynamic conditions using an orbital shaker at 37 °C for 4 weeks. The samples were then collected, rinsed with distilled water and dried in a vacuum oven for 24 hours. The surfaces of the samples were analysed using a UHR FE-SEM Hitachi SU8020, equipped with energy dispersive X-ray spectroscopy (EDX). An ultra-thin coating of chromium (Cr) with a thickness of 20 nm was applied to the samples using Quorum Q150T sputtering to provide electrical conductivity for the SEM.

https://doi.org/10.26434/chemrxiv-2024-6nlfd **ORCID:** https://orcid.org/0000-0001-9807-964X Content not peer-reviewed by ChemRxiv. **License:** CC BY 4.0

2.2.16. Water contact angle measurement

The surface wettability of copolymers was determined by measuring the water contact angle using a Krüss DSA 100 Drop Shape Analyser goniometer. The measurement was according to according to European Standard EN 828. The samples were prepared as dried films with a clean surface. A droplet of 2 µL of ultrapure deionised water was slowly dripped onto the surface of the sample, and after 1 min, a picture of the sessile drop was photographed using a macro lens. The contact angle was calculated by measuring 2 angles (left and right) from 5 separate sessile drops for each material.

2.2.17. Cytotoxicity

The cytotoxicity study was carried out according to ISO10993-5 using extract materials and the L292 cell line. Briefly, a 96-well plate was used to culture 10 x 10^3 of L292 cells in each well using complete growth medium (Dulbecco's Modified Eagle Medium (DMEM), containing 10% Fetal Bovine Serum (FBS), 2 mM L-glutamine, 100 U/mL penicillin and 100 µg/mL streptomycin). The cells were incubated for 24 hours at 37 °C in a CO_2 incubator. At the same time, samples films (0.5 mm thick) with a surface area of 3 cm^2 were prepared, cut into small pieces and placed in a 24-well plate. They were incubated in CO_2 incubator over 24 hours at 37 °C in 1ml of complete growth medium. Commercial, non-toxic poly(ε-caprolactone) (PCL, Capa™ 6430) was used as a negative control, nitrile glove (Mercator Nitrylex Classic, Kraków, Poland) were used as a positive control, no material as a control and media in empty well as a sham. After 24 h, the cell culture medium was aspirated from the plate and replaced with 100 µL of extract medium from a given sample (5 technical replicates; 3 samples per material). The plates were then returned to the cell culture incubator for a further 24 hours of culture.

3. Results and discussion

3.1. Visualisation of filler dispersion in polymer matrix

At the start of the research, the dispersion of filler particles in the composites was assessed. Figure 2 shows SEM images taken on cross-sections of rectangular composite specimens used for the impact test measurements.

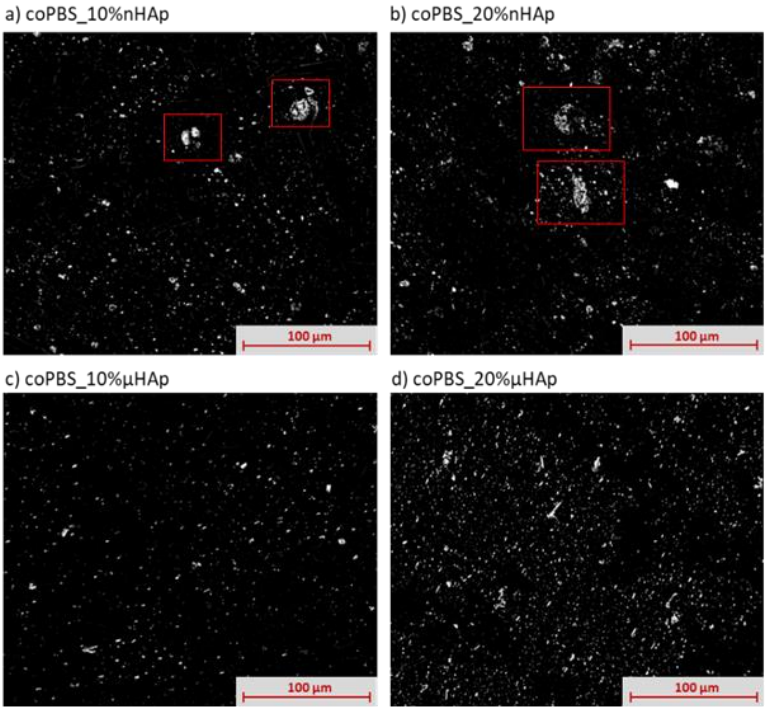

Figure 2. SEM images of the manufactured composites, registered on the cross-section of samples for impact tests. Magn. 1000×. Rectangular frames visible in pictures 'a' and 'b' indicate agglomerates of nanoparticles.

https://doi.org/10.26434/chemrxiv-2024-6nlfd **ORCID:** https://orcid.org/0000-0001-9807-964X Content not peer-reviewed by ChemRxiv. **License:** CC BY 4.0

Images 'a' and 'b' show the morphology of PBS-DLS composites with the addition of 10% and 20% by weight of nano-hydroxyapatite, respectively. As can be seen from the figure, the nanoparticles have a strong tendency to agglomerate. This tendency was already evident on the pre-process powder (Figure 1a). The problem of agglomeration of HAp nanoparticles in PBS-based composites has already been noted by Wenmin Guo [15]. Insufficient dispersion of the filler can affect the functional properties of the materials. The situation is different in the case of coPBS_10%µHAp and coPBS_20%µHAp composites. The microparticles do not show a clear tendency to agglomerate as in the pre-process powder (Figure 1b). Figure 2d shows the elongated shape of some HAp particles can be seen. However, there are only few of these, because during the process of filling the injection mould, the particles orient themselves parallel to the flow direction of the material, i.e. along the jet direction. Therefore, when viewed in section, the image shows whiskers from the 'base'. A more detailed analysis of the particle size in the composites was supported by particle size distribution studies.

3. 2. Particle size distribution

The methodology used for composite's manufacturing is based on melt mixing processes. On the one hand, this is a well-established approach derived from industrial techniques [24,27]. On the other hand, during these processes, the molten polymer is subjected to significant thermal (elevated temperature) and mechanical (shear forces between the material, screws, and the extruder barrel) stresses. Our previous work [24] demonstrates that such stresses in the system can lead to the cracking of apatite microfibres during processing. In this study, we attempt to quantify this phenomenon for the first time. For this purpose, we analysed the particle size distribution of the initial apatite fillers and then reassessed it in the final produced materials. The results of the quantitative analysis are presented in Figure 3. The example SEM images used for the calculations are provided in Supplementary Figure S2.

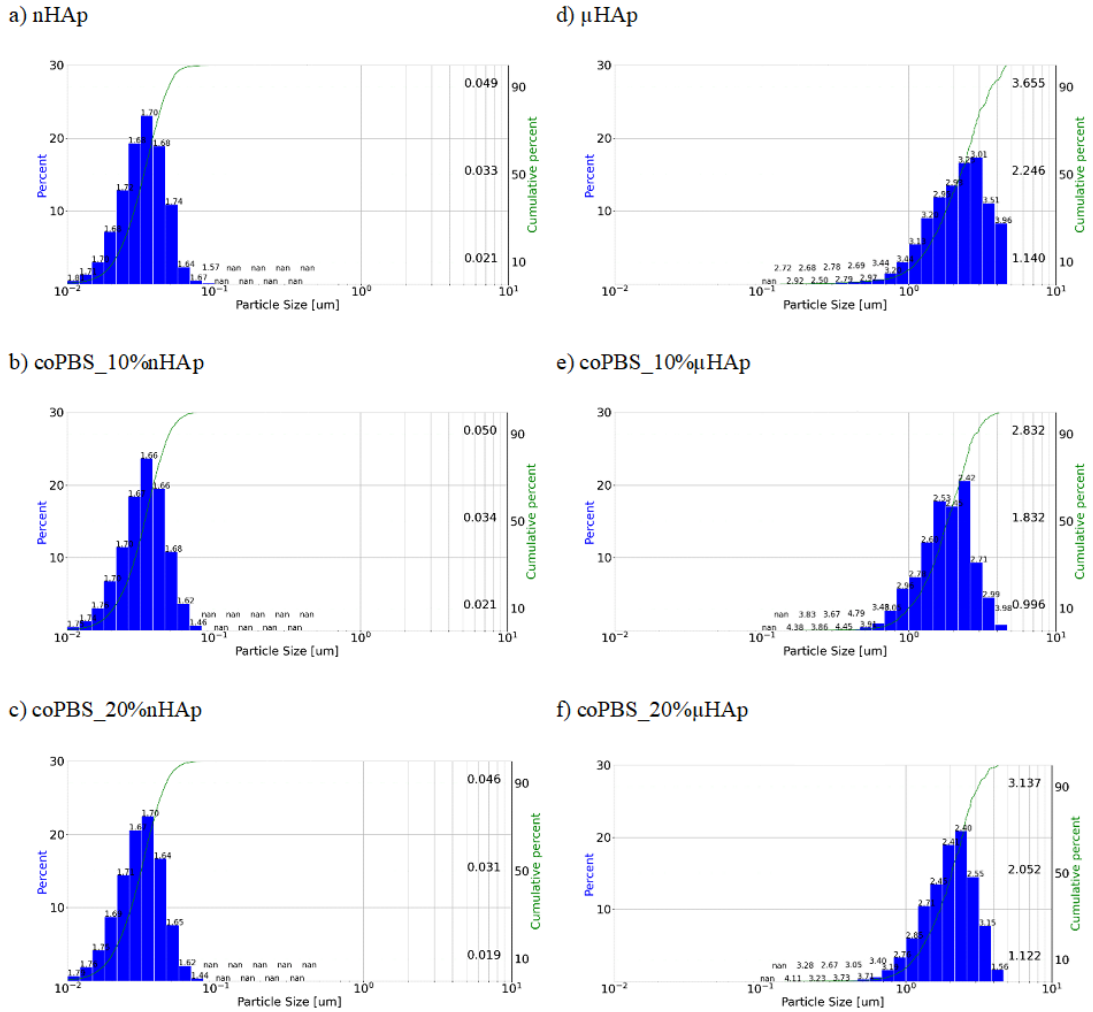

Figure 3. Particle size distribution curves: a, d - for starting powders, b, c, e, f - for particles in composites.

https://doi.org/10.26434/chemrxiv-2024-6nlfd **ORCID:** https://orcid.org/0000-0001-9807-964X Content not peer-reviewed by ChemRxiv. **License:** CC BY 4.0

The two powders used as a sources of hydroxyapatite are characterised by very different particle size distributions. The 'nano' form of hydroxyapatite (nHAp) contains grains no larger than 100 nm (d_{10} = 0.021 µm, d_{50} = 0.033 µm, d_{90} = 0.049 µm), whereas the 'micro' form of hydroxyapatite (µHAp) contains grains larger than 1 µm (d_{10} = 1.140 µm, d_{50} = 2.246 µm, d_{90} = 3.655 µm). Another important difference is the aspect ratio (AR) of the particles. The 'micro' form is characterised by much more elongated grains (AR greater than 3.0 - in most cases around 4.0), whereas the 'nano' type has much more spherical grains (AR below 1.7).

Analysing the particle size distributions in the composites with the addition of µHAp (Figures 3E and 3F), a reduction in the number of larger grains can be observed. This is due to the previously mentioned fact that, during the composite preparation process, the material is subjected to significant thermal and mechanical stresses, which cause fibre breakage. As a result, the aspect ratio decreases from nearly 4.0 to less than 3.0, and the d_{90} decreases from 3.65 mm to 2.83 mm when comparing the grains in the powder to those included in the composite. The observed reduction in particle size occurs to a similar extent for the coPBS_10%µHAp and coPBS_20%µHAp composites. The phenomenon of whisker length reduction (which, due to their shape, have the potential to reinforce the material [28]), together with the appearance of smaller particle size fractions, may negatively affect the reinforcing effect of HAp grains on the material. For the 'nano' type this phenomenon is not observed, and both AR and d_{90} remain at the similar levels. The above analyses assume that the apatite particles remain thermally stable at the static calcination temperature and that their geometry does not change significantly.

3.3. Gel permeation chromatography, density

Table 2 summarises the number average molecular weight (M_n) and weight average molecular weight (M_w) of the polymer in the produced materials. Analysis of the M_n and M_w parameters shows that their values increase with higher filler content in the composite. This trend is particularly evident in samples containing micro-hydroxyapatite. This can be explained by the fact that HAp, as a ceramic material with a higher heat capacity than the polymer, absorbs some of the heat generated during processing, thus limiting polymer degradation. As a result, the molecular weight of the reference sample without filler reaches the lowest values, since the pure polymer undergoes the greatest degradation. Table 2 also shows the absolute density values determined for the materials tested. As expected, the density of the material increases as the denser filler content increases. Irrespective of the type of hydroxyapatite, this increase is similar, indicating that the processing method used allowed the production of composites with comparable mass fractions. This is further supported by the TGA measurements.

Table 2. Average values of *M_n*, *M_w*, *DPI* index and absolute density for the reference coPBS and composite samples.

Sample	*M_n* [g/mol]	*M_w* [g/mol]	*DPI* [-]	Density [g/cm^3]
coPBS	39747	143770	3.6	1.203 ± 0.013
coPBS_10%nHAp	39125	149446	3.8	1.282 ± 0.011
coPBS_20%nHAp	n.d.	n.d.	n.d.	1.363 ± 0.006
coPBS_10%µHAp	42724	151158	3.5	1.285 ± 0.012
coPBS_20%µHAp	45790	151098	3.3	1.379 ± 0.010

M_n – number average molecular weight, M_w – weight average molecular weight, DPI – polydispersity index.

3.4. Melt Mass-Flow Rate

The MFR is a useful parameter that provides information on the suitability of a given material for thermal processing. Figure 4 shows the values of the MFR index for each of the materials at two stages of processing - after extrusion process and after injection moulding.

When analysing the results obtained, two main trends can be observed. The first one is visible within the limits of a given sample - with the next processing stage, the MFR value increases slightly. This is due to the fact

https://doi.org/10.26434/chemrxiv-2024-6nlfd **ORCID:** https://orcid.org/0000-0001-9807-964X Content not peer-reviewed by ChemRxiv. **License:** CC BY 4.0

that each of the processing steps (extrusion, injection) is inextricably linked to high thermomechanical stresses that cause polymer degradation. Numerous scientific studies show that the decrease in the molecular weight of the polymer is associated with a decrease in its viscosity, and thus an increase in the mass flow rate [29]. This observation is consistent with the polymer molecular weight values shown in Table 2.

The second of the observed trends is manifested by a decrease in the MFR index (increase in viscosity) in proportion to the filler content. This phenomenon has also been described in the scientific literature. Othman Y Alothman et al. show in their publication that the addition of HAp significantly reduces the melt flowability of the material [30].

Comparing the effect of nHAp and μHAp on the MFR value, it can be seen that nHAp reduces it much more. In the case of the coPBS_20%nHAp sample, its values decrease by up to 50%, while for the coPBS_20%μHAp sample it decreases by about 30%. The reason should be sought in the much higher value of specific surface area in the case of nHAp particles. Their interaction with the polymer matrix is much greater than in the case of HAp whiskers. Thus, for materials containing nHAp, the flow of the material in the plastic state is hindered, which may result in poorer processing properties.

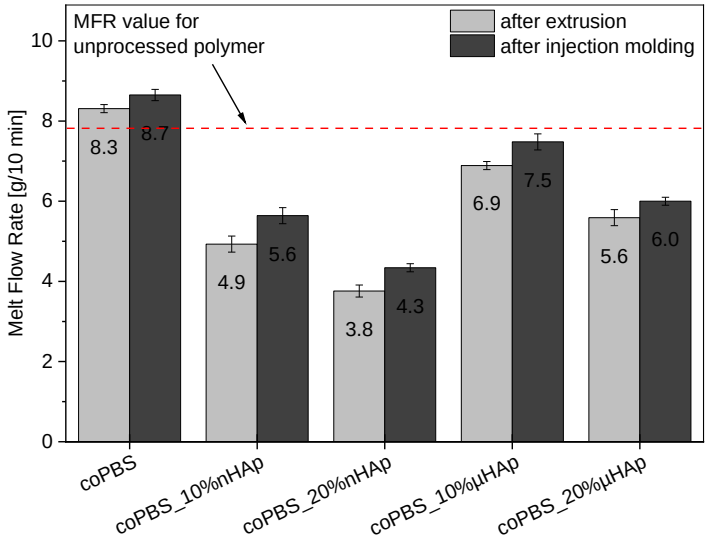

Figure 4. MFR values of the tested samples determined for materials after the extrusion process and after the injection molding process.

3.5. Thermal properties

Thermogravimetry analysis

The thermal behaviour of the composites was investigated during TG-DTA experiments in the inert atmosphere of argon. The recorded TGA thermograms (Figure 5) indicate that the materials have relatively high thermal stability, as their maximum decomposition step occurs at temperatures ranging between 394 °C and 402 °C. The main mass loss step (78–99 wt%) was observed in the temperature range of 260–485 °C, and the high temperature decomposition takes place above 485 °C with a mass loss of about 1 wt%. The course of the DTG curves (Figure S3) suggests that simultaneous processes occur during heating of the material, and therefore a weak signal can be observed around 448 °C.

For temperatures at 5 wt% and 10 wt% loss of mass, corresponding to the thermal stability of the material, it was observed that filler addition had a positive effect, except for 20% nHAp addition for which no improvement in these parameters was observed. The DTG extremum signals for the composites showed slightly lower values than for the unfilled material. The solid residue after the TGA experiment corresponds to the amount of the filler in the composition as shown in Table 3, which once again confirms the effectiveness of the chosen processing route [24].

https://doi.org/10.26434/chemrxiv-2024-6nlfd **ORCID:** https://orcid.org/0000-0001-9807-964X Content not peer-reviewed by ChemRxiv. **License:** CC BY 4.0

Comparison of TG curves for pure fillers and composites calcined at 500 °C shows that fillers lose approximately 2.4 wt% (μHAp) and 4.7 wt% (nHAp) of mass up to the temperature corresponding to the total degradation of the polymer matrix. The results obtained are in good agreement with previous reports, which showed that the maximum degradation rate of poly(alkylene succinates) reached 430 °C. It has been reported that during degradation mainly vinyl- and carboxyl-terminated compounds are produced and to a lesser extent aldehydes [31].

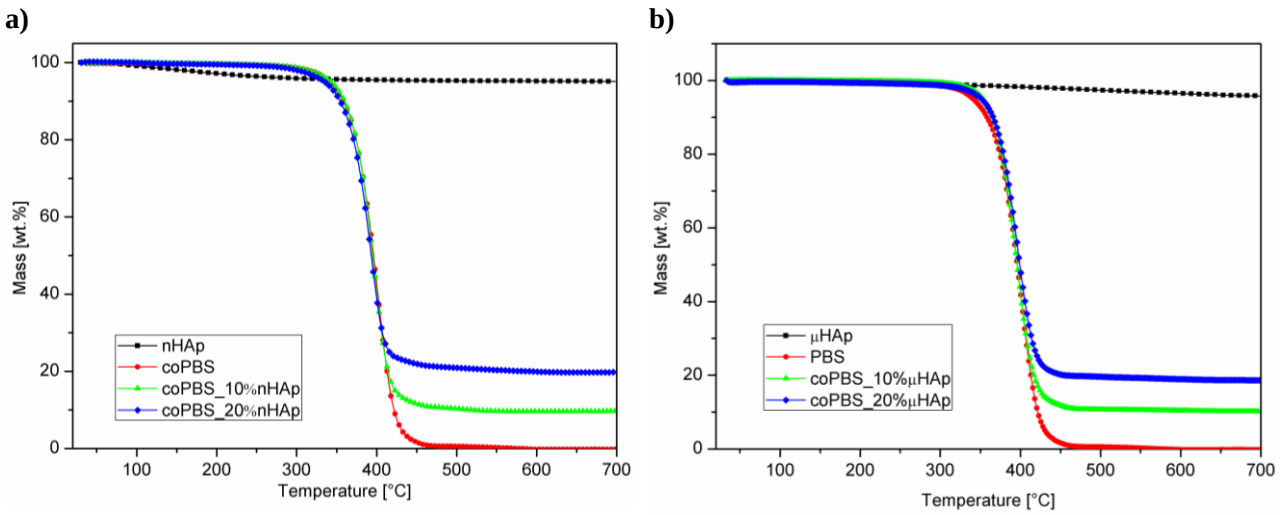

Figure 5. Analysis of the thermal stability of materials a - based on nHAp, b - based on μHAp in relation to the starting HAp powders and the coPBS reference sample.

Table 3. Thermal parameters evaluated by means of TG/DTA ($T_{\%}$ – temperature at 5% and 10% of mass loss, respectively; T_{dtg} – temperature at DTG extremum, T_{dta} – temperature at DTA extremum).

Sample	$T_{5\%}$ (°C)	$T_{10\%}$ (°C)	Solid residue (wt. %)	T_{dtg} (°C)	T_{DTA} (°C)
coPBS	341	358	–	402	112
coPBS_10%nHAp	343	360	9.65	397	109
coPBS_20%nHAp	335	354	19.77	394	108
coPBS_10%μHAp	353	365	10.21	396	110
coPBS_20%μHAp	351	366	18.62	397	109

Differential Scanning Calorimetry analysis

Understanding of phase transformations that occur in the polymer as a result of temperature changes is extremely important in the context of planning and designing the processing of polymeric materials. The effect of HAp powder addition on the thermal properties of the PBS-DLS copolymer was investigated using the DSC technique. In addition to understanding the nature of the materials produced, the purpose of the calorimetric studies was to compare the effect of the addition of nHAp and μHAp fillers on the thermal properties of the copolymer. Figure 6 shows the second heating DSC thermograms of the materials tested, while Figure 7 shows the first cooling thermograms. The parameters obtained from these data are summarised in Table 4.

Analysis of the calorimetric curves in Figure 6 shows that in all cases there is a slight inflection related to the glass transition of the polymer. In all cases, the inflection point, which can be interpreted as the glass transition temperature T_g is in a similar temperature range of 38-40 ºC, with no particular relationship to the filler content. In the temperature range of about 50-120 ºC, a clear endothermic effect can be observed, characteristic of the melting of semi-crystalline domains originating from the so-called 'hard segment' of the polymer chain (PBS block) [11]. The melting effect recorded has a bimodal distribution in all cases, indicating the presence of two types of crystallites in the system. This fact is not directly related to the presence of HAp particles in the system, as it can also be observed in the reference sample coPBS. This phenomenon can be the subject of separate studies. The melting point T_m was determined as the maximum of the predominant peak and differs

https://doi.org/10.26434/chemrxiv-2024-6nlfd ORCID: https://orcid.org/0000-0001-9807-964X Content not peer-reviewed by ChemRxiv. License: CC BY 4.0

slightly for all materials and is in the range of 106.9 ºC - 107.7 ºC. It should also be noted that such a wide melting range of the material can lead to instability of the material properties already from about 40 ºC for some samples. Calculations of the degree of crystallinity showed no significant influence of the hydroxyapatite filler on the crystallinity of the copolymer.

Figure 7 presents the DSC cooling thermograms. The exothermic effect visible on them is related to the process of crystallisation of the polymer from the melt. A significant difference in the crystallisation parameters compared to the other materials can be see especially for the coPBS_20%nHAp sample. It is worth noting that the apatite particles introduced into the PBS-DLS copolymer did not show any clear nucleation effect on the crystallisation phenomenon.

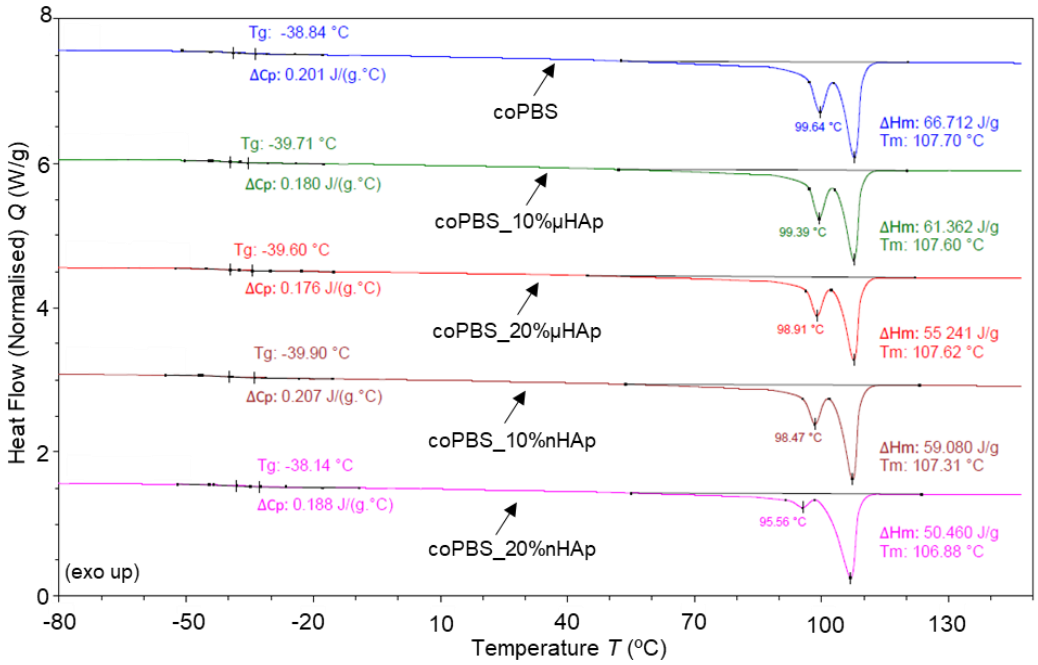

Figure 6. DSC calorimetric curves of the reference coPBS and the composite coPBS/HAp samples – 2nd heating scan.

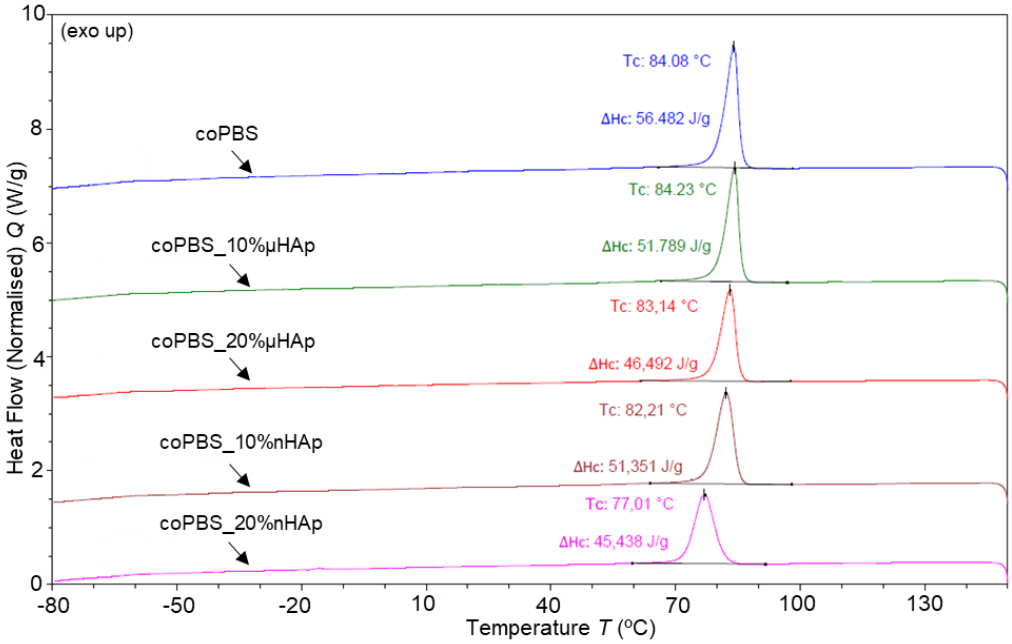

Figure 7. DSC calorimetric curves of the reference coPBS and the composite coPBS/HAp samples – 1st cooling scan.

https://doi.org/10.26434/chemrxiv-2024-6nlfd **ORCID:** https://orcid.org/0000-0001-9807-964X Content not peer-reviewed by ChemRxiv. **License:** CC BY 4.0

Table 4. A set of parameters determined from the DSC curves (Fig. 6, Fig. 7).

Sample	T_g [ºC]	ΔH_m [J/g]	T_m [ºC]	ΔH_c [J/g]	T_c [ºC]	X_c [%]
coPBS	-38.8	66.7	107.7	56.5	84.1	60.5
coPBS_10%nHAp	-39.9	59.1	107.3	51.4	82.2	59.5
coPBS_20%nHAp	-38.1	50.5	106.9	45.4	77.0	57.2
coPBS_10%µHAp	-39.7	61.4	107.6	51.8	84.2	61.9
coPBS_20%µHAp	-39.6	55.2	107.6	46.5	83.1	62.6

T_g – glass transition temperature, ΔH_m – enthalpy of melting, T_m – temperature of melting, ΔH_c – enthalpy of crystallization, T_c – temperature of crystallization, X_c – degree of crystallinity.

3.6. Dynamic mechanical thermal analysis

DMTA studies are an important complement to the results obtained from DSC measurements. They allow the observation of phase transformations, the determination of mechanical parameters, as well as the study of the viscoelastic properties of polymeric materials.

Figures 8a and 8b show the results of the temperature sweep experiment in terms of the storage modulus - E' (Fig. 8a) and the damping factor - tanδ (Fig. 8b) as a function of temperature.

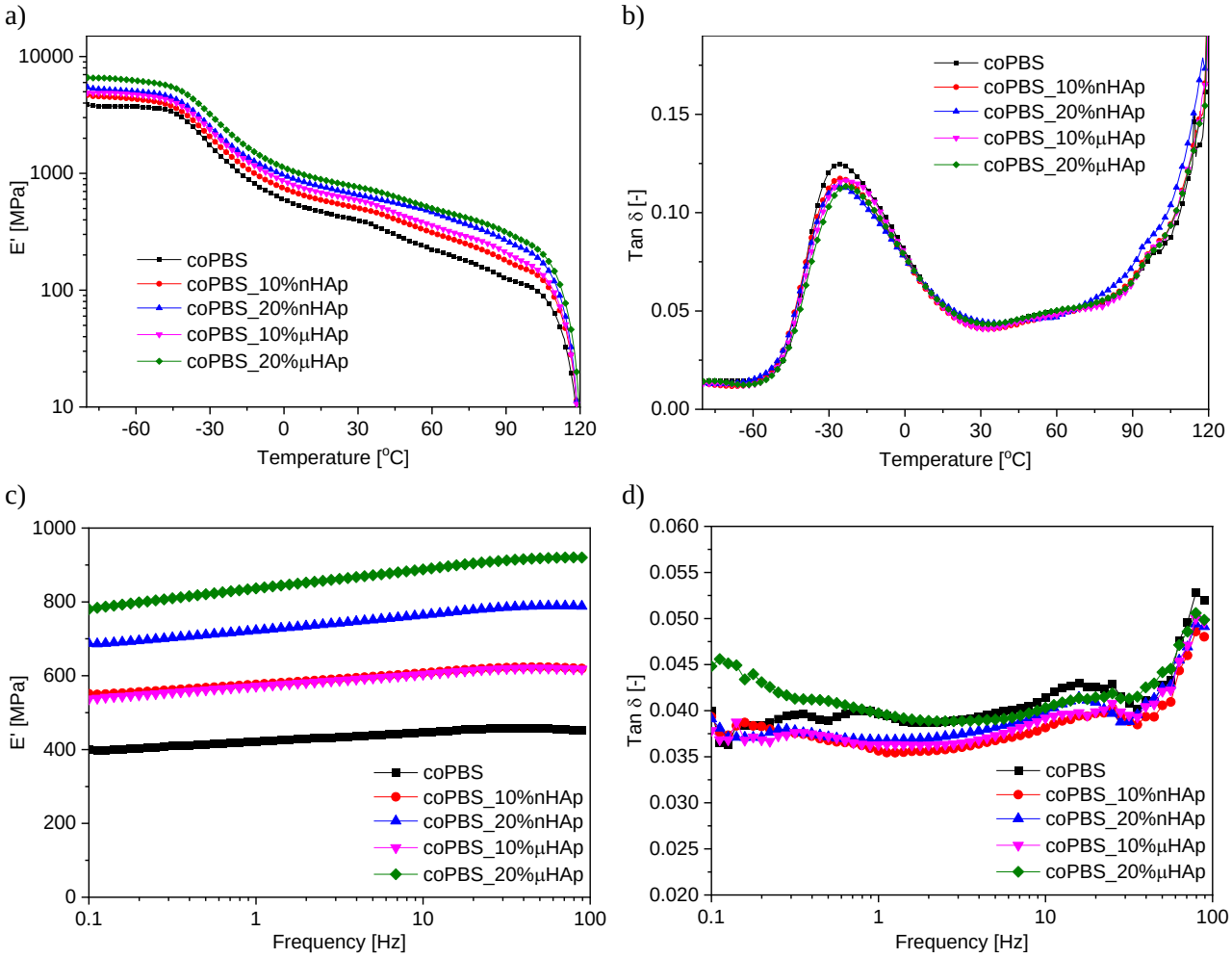

Figure 8. DMTA results: a, b – curves of storage moduli and damping factors versus temperature, c, d – curves of storage moduli and damping factors obtained during frequency sweep measurements.

The curves of E'(T) and tanδ(T) are very similar for all materials. In the temperature range of -60 ºC – 30 ºC, a clear decrease in the value of the storage modulus is observed, indicating the glass transition of the polymer. This is also indicated by the appearance of a distinct peak in Figure 8b. Table 3 summarises the values of the glass transition temperatures determined as the temperature corresponding to the maximum position of this

https://doi.org/10.26434/chemrxiv-2024-6nlfd **ORCID:** https://orcid.org/0000-0001-9807-964X Content not peer-reviewed by ChemRxiv. **License:** CC BY 4.0

peak. They are significantly higher than those obtained by DSC (Table 3) and range from -26.3 to 29.0 ºC. This difference is mainly due to the size of the samples. In the case of DMTA, although the heating rate is much lower than in DSC, the large dimensions of the samples mean that the heat penetrates the sample for a much longer time, which results in a delay in the change in the mechanical properties of the material. After the glass transition, a further decrease in the storage modulus is seen with a parallel increase in tanδ. This indicates an increase in the value of the loss modulus E", and thus an increased ratio of viscous properties to elastic properties of the material. The results obtained correlate well with the DSC results. A wide range of the melting effect translates into a rapid loss of the elastic properties of the material just above room temperature. Another correlation is the lack of obvious changes in the course of the curves and only cosmetic differences in the characteristics of the phase transitions.

The largest changes are observed in the direct values of the storage modulus, indicating differences in the mechanical properties of the materials. Table 4 shows the values of the E' parameter of the materials recorded at the temperature before the glass transition (T = -60 ºC), at room temperature - after the glass transition (T = 25 ºC) and at the temperature before the melting point of the material (T = 80 ºC). The trend is very similar at all the points shown. The E' modulus values are clearly increased in proportion to the filler content in the composite. Moreover, this reinforcement is clearly dependent on the type of filler. The µHAp particles allow a much higher reinforcement of the material than the nHAp particles. For example, the storage modulus determined for the coPBS_20%µHAp composite at room temperature is 90% higher than for coPBS, while for coPBS_20%nHAp it is only 64 % higher.

A frequency sweep experiment was performed to better understand the viscoelastic properties of the materials. Figures 8c and 8d show the dependence of *E'* and tanδ on the oscillation frequency, respectively. All materials have stable viscoelastic properties in the frequency range of 0.1 - 100 Hz. For all of them, the damping coefficient practically does not exceed 5%, confirming the elastic properties of the materials. In turn, the absolute values of the E' moduli again show the same trend as during the temperature sweep over the whole frequency range.

Table 4. Dynamic mechanical thermal parameters determined from DMTA curves.

Sample	Temperature sweep				Frequency sweep	
	E' [GPa] at -60 ºC	E' [GPa] at 25 ºC	E' [GPa] at 80 ºC	T_g [ºC]	E' [GPa] at 1 Hz	E'[GPa] at 10 Hz
coPBS	3.73	0.42	0.16	-29.0	0.42	0.45
coPBS_10%nHAp	4.32	0.53	0.22	-28.5	0.58	0.61
coPBS_20%nHAp	5.02	0.69	0.33	-29.0	0.72	0.76
coPBS_10%µHAp	4.72	0.62	0.26	-26.3	0.57	0.60
coPBS_20%µHAp	6.22	0.80	0.38	-26.5	0.84	0.89

3.7. Quasi-static mechanical analyses

Quasi-static tensile tests, quasi-static flexural tests, Charpy impact tests and Brinell hardness measurements were carried out to fully evaluate the mechanical properties of the manufactured composites.

Figure 9a shows representative stress-strain curves for each material. In turn, Figs. 9b-d show the parameters of strain at break, tensile modulus and tensile strength. All the mechanical parameters determined are listed in Table 5. As can be seen in Figure 9a, the addition of hydroxyapatite significantly affected the deterioration of the copolymer ductility. A similar phenomenon in PBS/nHAp composites was also observed by Wenmin Guo [15]. In Figure 9b, it can be seen that these decreases are greater for nHAp than for µHAp. The may be due to the tendency of nanoparticles to agglomerate, resulting in disruption of continuity and weakening of the polymer structure. In turn, Figures 9c and 9d again show the effect of filler addition on tensile modulus and tensile strength, and here the opposite phenomenon occurs - material strengthening. Regarding the tensile strength parameter, the highest reinforcement was obtained for the sample with 20% micro-hydroxyapatite content (about 17%). In turn, the analogous composite with nano-hydroxyapatite was only strengthened by

https://doi.org/10.26434/chemrxiv-2024-6nlfd **ORCID:** https://orcid.org/0000-0001-9807-964X Content not peer-reviewed by ChemRxiv. **License:** CC BY 4.0

only 6%. Similarly, in the case of the tensile modulus, apatite micro-whiskers showed a greater strengthening efficiency. The results obtained are consistent with literature reports indicating the particular strengthening potential of whisker-like HAp particles [32,33].

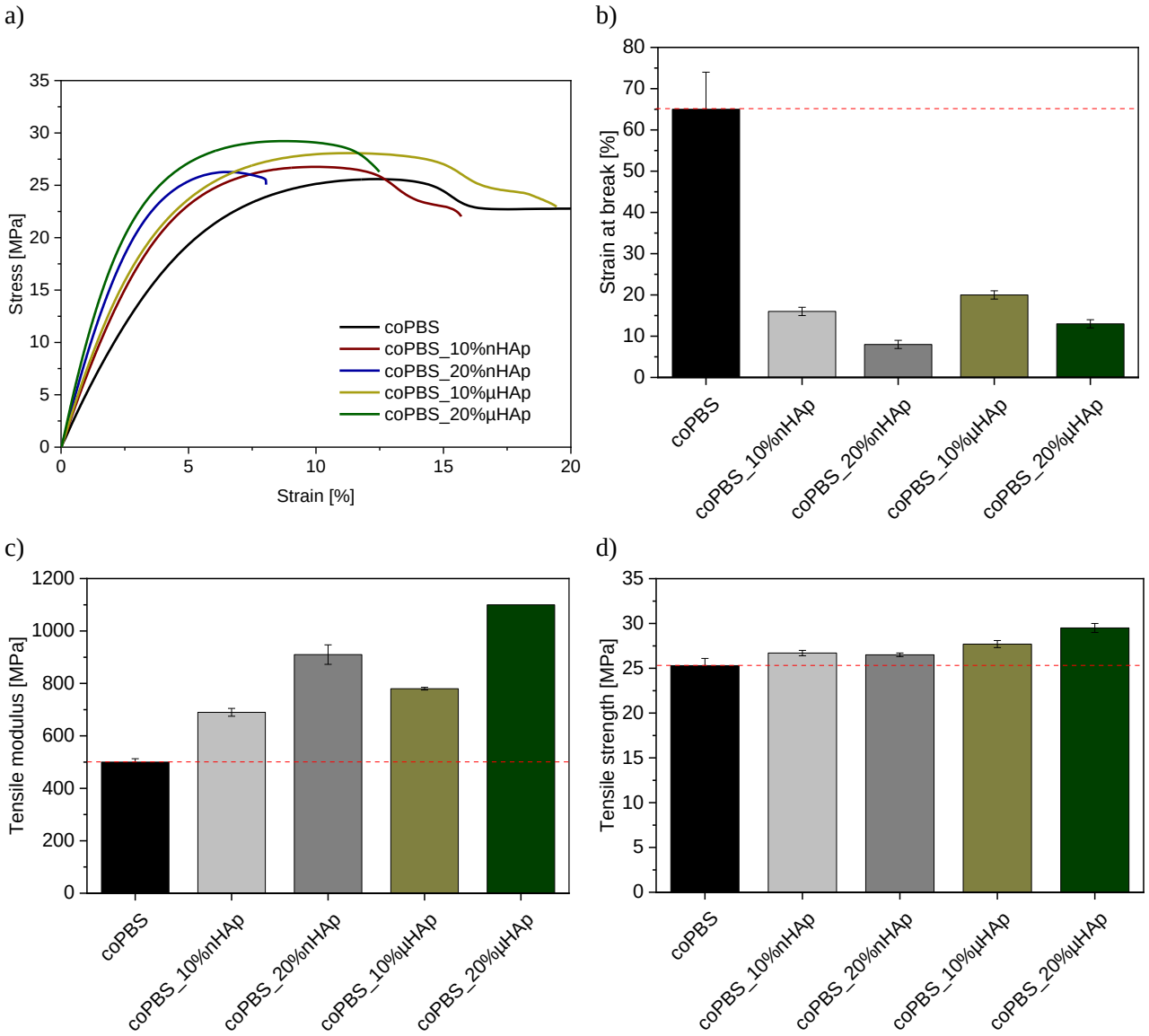

Figure 9. Static tensile mechanical properties of materials: a - representastive stress-strain curves obtained during static tensile test; b, c, d – strain at break, tensile modulus and tensile test parameters, respectively. The red dashed line refers to the parameter value of the coPBS reference sample.

The mechanical properties (flexural modulus, stress at 3.5% of strain) of the materials subjected to static bending were also significantly improved after the addition of the filler, but no major differences were observed between the PBS/DLS/nHAp and PBS/DLS/µHAp composites (Figures 10a, 10b).

For many polymers, even a small addition of the HAp filler is associated with a drastic reduction in the impact strength of the material [24,34]. The same is true for PBS/nHAp composites produced by extrusion and injection molding techniques [15]. As the filler content in the polymer-ceramic system increases, the filler particles agglomerate more and more, forming stress concentration points that lead to a significant weakening of the material. Now, it turns out that in the tested PBS-DLS/HAp materials, the addition of hydroxyapatite is even able to slightly strengthen the material against dynamic loads (Figure 10C - sample coPBS_10%nHAp). For the other samples, a weakening is observed, but it does not exceed 25 % compared to coPBS, which is quite good result.

https://doi.org/10.26434/chemrxiv-2024-6nlfd **ORCID:** https://orcid.org/0000-0001-9807-964X Content not peer-reviewed by ChemRxiv. **License:** CC BY 4.0

As expected, the filled samples are characterised by a higher hardness with respect to the reference, proportional to the addition of the filler. Composites with nano-hydroxyapatite are characterised by a higher hardness than their counterparts with micro-hydroxyapatite.

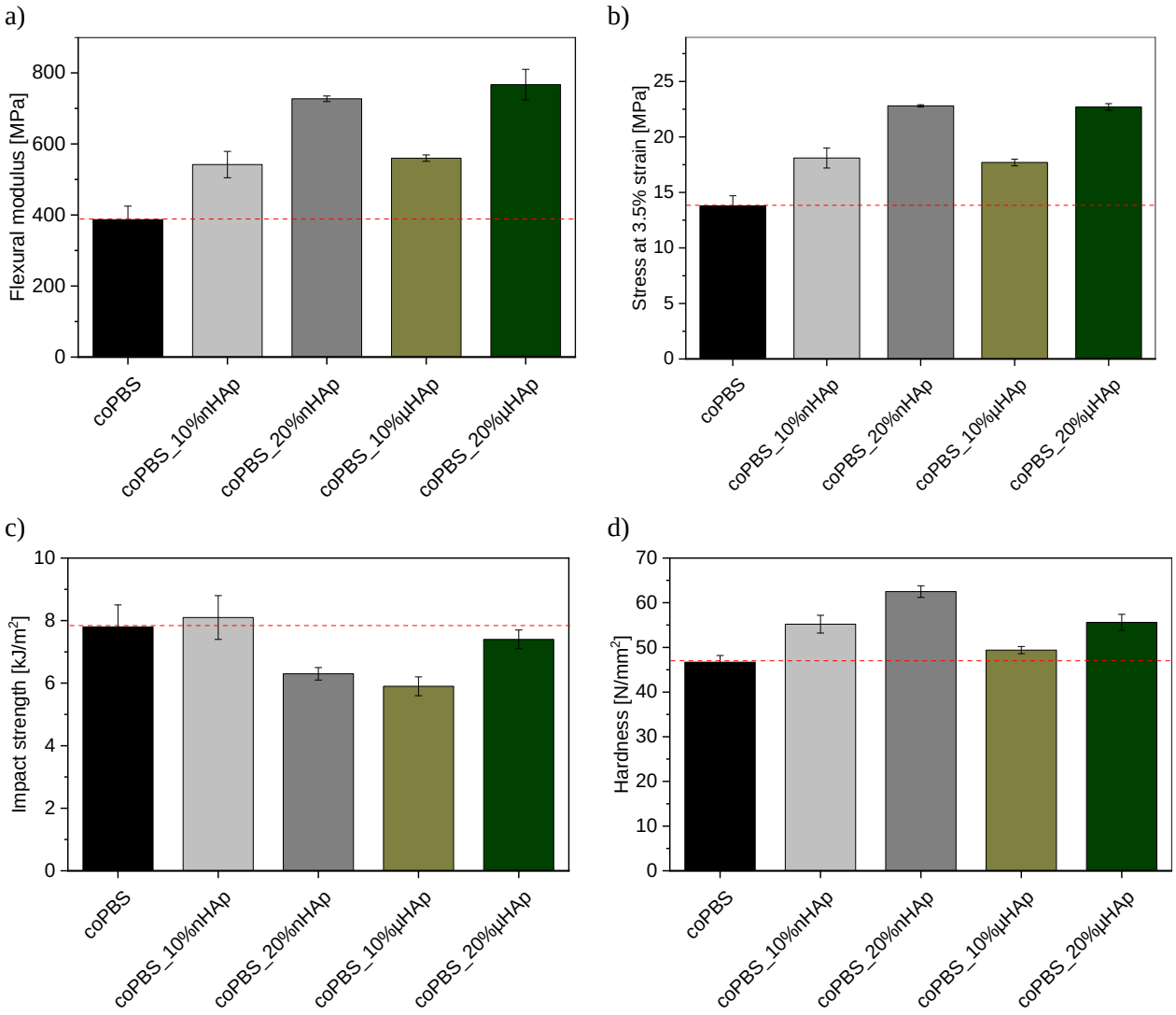

Figure 10. Mechanical parameters of tested materials: a – flexural modulus, b – stress at 3.5% strain, c – Charpy notched impact strength, Brinell hardness. The red dashed line refers to the parameter value of the coPBS reference sample.

Table 5. Selected mechanical parameters of the composites tested and the reference material.

Sample	*UTS* [MPa]	E_T [GPa]	ε_B [%]	E_B [GPa]	$\sigma_{\varepsilon=3.5\%}$ [MPa]	a_N [kJ/m²]	*HB* [N/mm²]
coPBS	25.3 ±0.8	0.50 ±0.01	65 ±9	0.39 ±0.04	13.8 ±0.9	7.8 ±0.7	46.7 ±1.5
coPBS_10%nHAp	26.7 ±0.3	0.69 ±0.02	16 ±1	0.54 ±0.04	18.1 ±0.9	8.1 ±0.7	55.2 ±2.0
coPBS_20%nHAp	26.5 ±0.2	0.91 ±0.04	8 ±1	0.73 ±0.01	22.8 ±0.1	6.3 ±0.2	62.5 ±1.3
coPBS_10%µHAp	27.7 ±0.4	0.78 ±0.01	20 ±1	0.56 ±0.01	17.7 ±0.3	5.9 ±0.3	49.4 ±0.8
coPBS_20%µHAp	29.5 ±0.5	1.10 ±0.01	13 ±1	0.77 ±0.04	22.7 ±0.3	7.4 ±0.3	55.6 ±1.8

UTS – ultimate tensile strength, E_T – tensile modulus, ε_B – strain at break, E_B – flexural modulus, $\sigma_{\varepsilon=3.5\%}$ = stress at 3.5% strain (bending), a_N – Charpy notched impact strength, *HB* – Brinell hardness.

https://doi.org/10.26434/chemrxiv-2024-6nlfd **ORCID:** https://orcid.org/0000-0001-9807-964X Content not peer-reviewed by ChemRxiv. **License:** CC BY 4.0

3.8. Biological activity assessment

The bioactivity of the tested materials was assessed by immersion in the SBF solution for 4 weeks, followed by a qualitative and quantitative analysis of their surface using the SEM/EDX technique. Figure 11 shows the SEM images of the analysed surfaces. As can be seen, nucleation and growth of mineral clusters, similar to the mineral fraction of bone, occurs on all surface examined. EDX analysis confirmed the presence of calcium, oxygen and phosphorus atoms in quantities corresponding to the structure of hydroxyapatite (Figure S4 – Supplementary Information). These results indicate that all of produced PBS-DLS/HAp composites have good biocompatibility and osteogenic capacity [16].

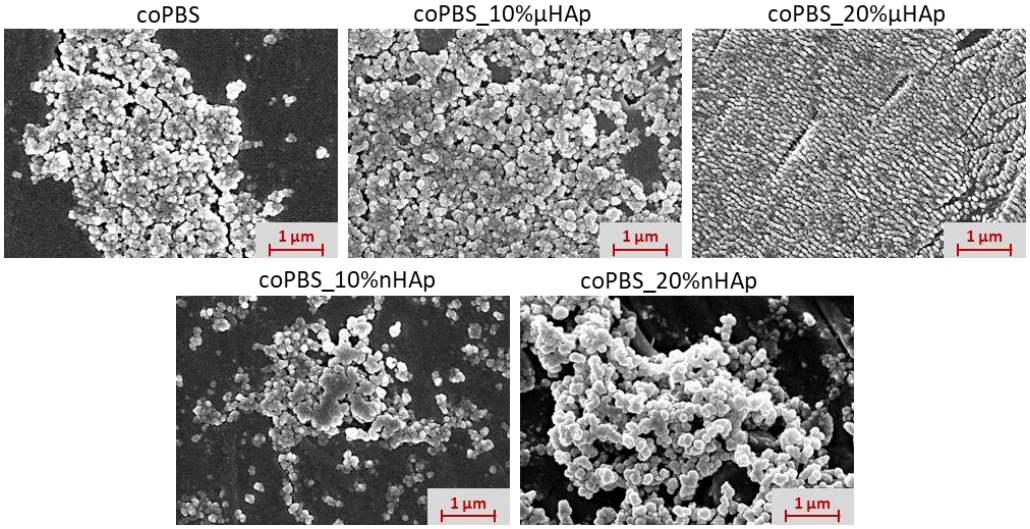

Figure 11. Bioactivity assessment - SEM images of the surface of materials incubated in SBF solution for 4 weeks.

3.9. Wettability

Surface wettability was tested by water droplet deposition and contact angle measurement. The PBS-DLS reference material is inherently hydrophobic. On the other hand, apatite ceramics have hydrophilic properties. By introducing the hydroxyapatites into the polymer matrix made it possible to reduce the contact angle by a value from the range of 9 - 12.8 degrees, depending on the material. No significant differences were observed between composites with nano- and microsized fillers.

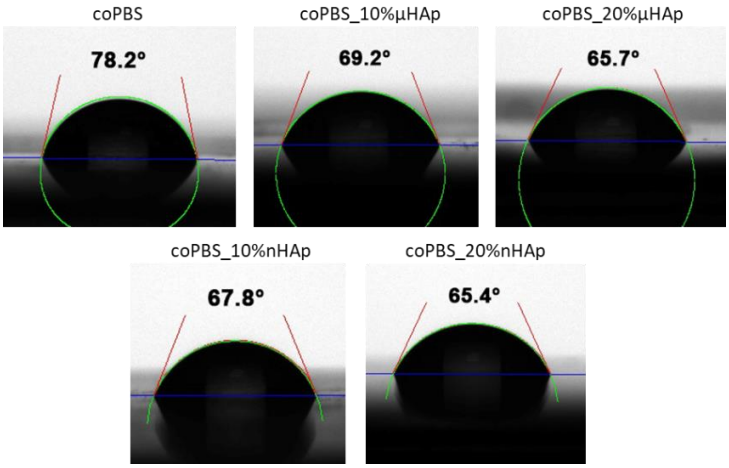

Figure 12. Surface wettability analysis - representative droplet images and averaged water contact angle values.

3.10. Cytotoxicity

The results of the cell viability assay results for L929 mouse fibroblasts exposed to extracts of the tested materials for 24 h are shown in Figure 13. The results indicated high cell viability for all materials tested, near 100% with no significant differences.

https://doi.org/10.26434/chemrxiv-2024-6nlfd **ORCID:** https://orcid.org/0000-0001-9807-964X Content not peer-reviewed by ChemRxiv. **License:** CC BY 4.0

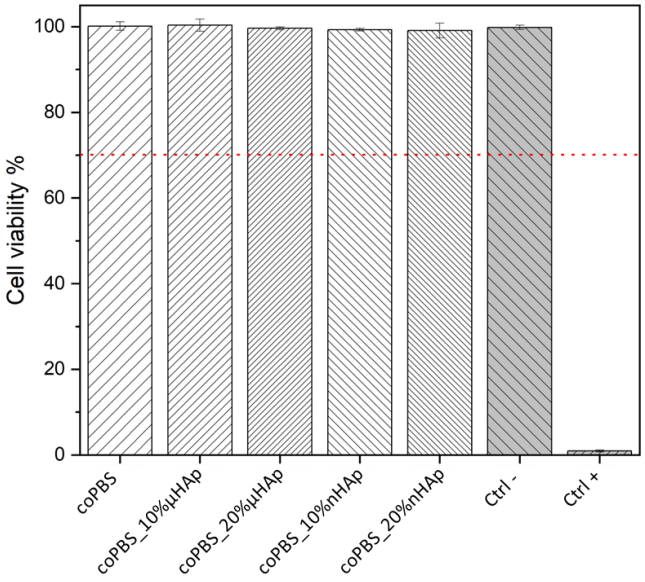

Figure 13. L929 cell viability after 24 h of exposure to extracts of materials obtained. The dashed line indicates the 70% cytotoxicity threshold according to ISO10993-5.

4. Conclusions

The paper presents novel polymer-ceramic composites based on PBS-DLS copolymer with the addition of hydroxyapatites of two different particle sizes (micro- and nano-hydroxyapatite). The materials were successfully prepared using co-rotating twin-screw extrusion and injection moulding techniques, with two copolymer-to-filler weight ratios (9:1 and 8:2) for each filler type.

The study investigates the influence of the applied manufacturing processes on the behaviour of the HAp filler particles in the composites. The nanoparticles show a strong tendency to agglomerate, while the whisker-shaped microparticles exhibit good dispersion within the PBS-DLS matrix. In addition, the processing methods do not significantly affect the size of the nanoparticles, but they do have a destructive effect on the whisker-shaped particles, reducing their aspect ratio from about 4 to less than 3 in the composites tested.

Various mechanical tests demonstrated the ability of the fillers to reinforce the PBS-DLS copolymer in proportion to their content. In dynamic thermo-mechanical tests and tensile tests, the strengthening was significantly more effective in composites with µHAp whiskers than with nHAp particles

Overall, the developed materials exhibited good processability, thermal stability, bioactivity and biocompatibility with the mouse fibroblast cell line L929, making them promising candidates for biomedical applications, particularly in bone tissue engineering.

Acknownledgements

This work has been financially supported by the Polish Ministry of Science and Higher Education for the Department of Chemistry at Wrocław University of Science and Technology through statutory funding no. 8211104160 (departmental code K23W03D05) and for Łukasiewicz Research Network - Institute of Ceramics and Building Materials through funding for ongoing activities (subsidy). This work has also received funding from the European Union's Horizon 2020 research and innovation program under the Marie Skłodowska-Curie grant agreement no. 872152 (GREEN MAP). An international project co-financed by the program of the Minister of Science and Higher Education entitled "PMW" in the years 2000-2023; contract No. 5091/H2020/2020/2 is acknowledged. Bartłomiej Kryszak is supported by the Foundation for Polish Science (FNP). The authors would also like to thank student Jan Urbański for his assistance in conducting part of the research.

https://doi.org/10.26434/chemrxiv-2024-6nlfd **ORCID:** https://orcid.org/0000-0001-9807-964X Content not peer-reviewed by ChemRxiv. **License:** CC BY 4.0

5. LITERATURE

[1] Mukherjee C, Varghese D, Krishna JS, Boominathan T, Rakeshkumar R, Dineshkumar S, et al. Recent advances in biodegradable polymers – Properties, applications and future prospects. Eur Polym J 2023;192:112068. https://doi.org/10.1016/j.eurpolymj.2023.112068.

[2] Samir A, Ashour FH, Hakim AAA, Bassyouni M. Recent advances in biodegradable polymers for sustainable applications. Npj Mater Degrad 2022;6. https://doi.org/10.1038/s41529-022-00277-7.

[3] Alaswad SO, Mahmoud AS, Arunachalam P. Recent Advances in Biodegradable Polymers and Their Biological Applications: A Brief Review. Polymers (Basel) 2022;14. https://doi.org/10.3390/polym14224924.

[4] Richbourg NR, Peppas NA, Sikavitsas VI. Tuning the biomimetic behavior of scaffolds for regenerative medicine through surface modifications. J Tissue Eng Regen Med 2019;13:1275–93. https://doi.org/10.1002/term.2859.

[5] Barletta M, Aversa C, Ayyoob M, Gisario A, Hamad K, Mehrpouya M, et al. Poly(butylene succinate) (PBS): Materials, processing, and industrial applications. Prog Polym Sci 2022;132:101579. https://doi.org/10.1016/j.progpolymsci.2022.101579.

[6] Dmitruk A, Ludwiczak J, Skwarski M, Makuła P, Kaczyński P. Influence of PBS, PBAT and TPS content on tensile and processing properties of PLA-based polymeric blends at different temperatures. J Mater Sci 2023;58:1991–2004. https://doi.org/10.1007/s10853-022-08081-z.

[7] Homklin R, Hongsriphan N. Mechanical and thermal properties of PLA/PBS cocontinuous blends adding nucleating agent. Energy Procedia 2013;34:871–9. https://doi.org/10.1016/j.egypro.2013.06.824.

[8] Kozlowska A, Gromadzki D, Fray M El, Štěpánek P. Morphology Evaluation of Biodegradable Copolyesters Based on Dimerized Fatty Acid Studied by DSC , SAXS and WAXS. Fibres & Textiles in Eastern Europe 2008;16:85–8.

[9] Kantor-Malujdy N, Skowron S, Michalkiewicz B, El Fray M. Poly(butylene-succinate)-based blends with enhanced oxygen permeability. Mater Today Commun 2022;33:104306. https://doi.org/10.1016/j.mtcomm.2022.104306.

[10] Stępień K, Miles C, McClain A, Wiśniewska E, Sobolewski P, Kohn J, et al. Biocopolyesters of Poly(butylene succinate) Containing Long-Chain Biobased Glycol Synthesized with Heterogeneous Titanium Dioxide Catalyst. ACS Sustain Chem Eng 2019;7:10623–32. https://doi.org/10.1021/acssuschemeng.9b01191.

[11] Zarei M, El Fray M. Synthesis of hydrophilic poly(Butylene succinate-butylene dilinoleate) (PBS-DLS) copolymers containing poly(ethylene glycol) (PEG) of variable molecular weights. Polymers (Basel) 2021;13. https://doi.org/10.3390/polym13183177.

[12] Saffian HA, Yamaguchi M, Ariffin H, Abdan K, Kassim NK, Lee SH, et al. Thermal, physical and mechanical properties of poly(Butylene succinate)/kenaf core fibers composites reinforced with esterified lignin. Polymers (Basel) 2021;13. https://doi.org/10.3390/polym13142359.

[13] Platnieks O, Gaidukovs S, Barkane A, Gaidukova G, Grase L, Thakur VK, et al. Highly loaded cellulose/poly (butylene succinate) sustainable composites for woody-like advanced materials application. Molecules 2020;25. https://doi.org/10.3390/molecules25010121.

[14] Motloung MP, Mofokeng TG, Bandyopadhyay J, Ray SS. Properties and Soil Degradation Characteristics of Chitin-Reinforced Poly(butylene succinate)/Hydroxyapatite Composites. Macromol Mater Eng 2024;309:1–12. https://doi.org/10.1002/mame.202300293.

https://doi.org/10.26434/chemrxiv-2024-6nlfd **ORCID:** https://orcid.org/0000-0001-9807-964X Content not peer-reviewed by ChemRxiv. **License:** CC BY 4.0

[15] Guo W, Zhang Y, Zhang W. Mechanical properties and crystallization behavior of hydroxyapatite/ poly(butylenes succinate) composites. J Biomed Mater Res A 2013;101 A:2500–6. https://doi.org/10.1002/jbm.a.34552.
[16] Li G, Qin S, Liu X, Zhang D, He M. Structure and properties of nano-hydroxyapatite/poly(butylene succinate) porous scaffold for bone tissue engineering prepared by using ethanol as porogen. J Biomater Appl 2019;33:776–91. https://doi.org/10.1177/0885328218812486.
[17] Prowans P, Kowalczyk R, Wiszniewska B, Czapla N, Bargiel P, El Fray M. Bone Healing in the Presence of a Biodegradable PBS-DLA Copolyester and Its Composite Containing Hydroxyapatite. ACS Omega 2019;4:19765–71. https://doi.org/10.1021/acsomega.9b02539.
[18] Roeder RK, Converse GL, Kane RJ, Yue W. Hydroxyapatite-reinforced polymer biocomposites for synthetic bone substitutes. JOM 2008;60:38–45. https://doi.org/10.1007/s11837-008-0030-2.
[19] Roohani-Esfahani SI, Nouri-Khorasani S, Lu Z, Appleyard R, Zreiqat H. The influence hydroxyapatite nanoparticle shape and size on the properties of biphasic calcium phosphate scaffolds coated with hydroxyapatite-PCL composites. Biomaterials 2010;31:5498–509. https://doi.org/10.1016/j.biomaterials.2010.03.058.
[20] Sharafeddin F, Feizi N. Evaluation of the effect of adding micro-hydroxyapatite and nano-hydroxyapatite on the microleakage of conventional and resin-modified Glass-ionomer Cl V restorations. J Clin Exp Dent 2017;9:e242–8. https://doi.org/10.4317/jced.53216.
[21] Munarin F, Petrini P, Gentilini R, Pillai RS, Dirè S, Tanzi MC, et al. Micro- and nano-hydroxyapatite as active reinforcement for soft biocomposites. Int J Biol Macromol 2015;72:199–209. https://doi.org/10.1016/j.ijbiomac.2014.07.050.
[22] Lebre F, Sridharan R, Sawkins MJ, Kelly DJ, O'Brien FJ, Lavelle EC. The shape and size of hydroxyapatite particles dictate inflammatory responses following implantation. Sci Rep 2017;7:1–13. https://doi.org/10.1038/s41598-017-03086-0.
[23] Kang X, Zhang W, Yang C. Mechanical properties study of micro- and nano-hydroxyapatite reinforced ultrahigh molecular weight polyethylene composites. J Appl Polym Sci 2016;133:1–9. https://doi.org/10.1002/app.42869.
[24] Kryszak B, Biernat M, Tymowicz-Grzyb P, Junka A, Brożyna M, Worek M, et al. The effect of extrusion and injection molding on physical , chemical , and biological properties of PLLA / HAp whiskers composites. Polymer (Guildf) 2023;287:126428. https://doi.org/10.1016/j.polymer.2023.126428.
[25] Sokołowska M, Nowak-Grzebyta J, Stachowska E, El Fray M. Enzymatic Catalysis in Favor of Blocky Structure and Higher Crystallinity of Poly(Butylene Succinate)-Co-(Dilinoleic Succinate) (PBS-DLS) Copolymers of Variable Segmental Composition. Materials 2022;15. https://doi.org/10.3390/ma15031132.
[26] Kokubo T, Kushitani H, Sakka S, Kitsugi T, Yamamuro T. Solutions able to reproduce in vivo surface-structure changes in bioactive glass-ceramic A-W3. J Biomed Mater Res 1990;24:721–34. https://doi.org/10.1002/jbm.820240607.
[27] Aniulis J, Kryszak B, Grzymajło M, Dudzik G, Abramski KM, Szustakiewicz K. Characterisation and manufacturing methods of material extrusion 3D printing composites filaments based on polylactide and nanohydroxyapatite. Engineering Archive 2024. https://doi.org/https://doi.org/10.31224/3783.

https://doi.org/10.26434/chemrxiv-2024-6nlfd **ORCID:** https://orcid.org/0000-0001-9807-964X Content not peer-reviewed by ChemRxiv. **License:** CC BY 4.0

[28] Li W, Lu Y, Liu K, Wen W, Liu M, Li H, et al. Preparation of HAp whiskers with or without Mg ions and their effects on the mechanical properties and osteogenic activity of poly(D,L-lactide). Compos B Eng 2020;196:108137. https://doi.org/10.1016/j.compositesb.2020.108137.
[29] Cheng Y-L, Lee C-Y, Huang Y-L, Buckner CA, Lafrenie RM, Dénommée JA, et al. Effect of Processing and Orientation on Structural and Mechanical Properties of Polypropylene Products. vol. 11. 2016. https://doi.org/DOI: http://dx.doi.org/10.5772/intechopen.85554.
[30] Alothman OY, Fouad H, Al-Zahrani SM, Eshra A, Al Rez MF, Ansari SG. Thermal, creep-recovery and viscoelastic behavior of high density polyethylene/hydroxyapatite nano particles for bone substitutes: Effects of gamma radiation. Biomed Eng Online 2014;13:1–15. https://doi.org/10.1186/1475-925X-13-125.
[31] Bikiaris RD, Ainali NM, Christodoulou E, Nikolaidis N, Lambropoulou DA, Papageorgiou GZ. Thermal Stability and Decomposition Mechanism of Poly(alkylene succinate)s. Macromol 2022;2:58–77. https://doi.org/10.3390/macromol2010004.
[32] Converse GL, Conrad TL, Merrill CH, Roeder RK. Hydroxyapatite whisker-reinforced polyetherketoneketone bone ingrowth scaffolds. Acta Biomater 2010;6:856–63. https://doi.org/10.1016/j.actbio.2009.08.004.
[33] Roeder RK, Sproul MM, Turner CH. Hydroxyapatite whiskers provide improved mechanical properties in reinforced polymer composites. J Biomed Mater Res A 2003;67:801–12. https://doi.org/10.1002/jbm.a.10140.
[34] Akindoyo JO, Beg MDH, Ghazali S, Heim HP, Feldmann M. Effects of surface modification on dispersion, mechanical, thermal and dynamic mechanical properties of injection molded PLA-hydroxyapatite composites. Compos Part A Appl Sci Manuf 2017;103:96–105. https://doi.org/10.1016/j.compositesa.2017.09.013.

https://doi.org/10.26434/chemrxiv-2024-6nlfd **ORCID:** https://orcid.org/0000-0001-9807-964X Content not peer-reviewed by ChemRxiv. **License:** CC BY 4.0